AIP | Journal of Applied Physics

Qualitative and quantitative evaluation of thin-film solar cells using solar cell local characterization

J.-M. Wagner, J. Carstensen, A. Schütt, and H. Föll

Citation: J. Appl. Phys. **113**, 064503 (2013); doi: 10.1063/1.4790479
View online: http://dx.doi.org/10.1063/1.4790479
View Table of Contents: http://jap.aip.org/resource/1/JAPIAU/v113/i6
Published by the American Institute of Physics.

Qualitative and quantitative evaluation of thin-film solar cells using solar cell local characterization

J.-M. Wagner, J. Carstensen,[a] A. Schütt, and H. Föll
Institute for General Materials Science, Faculty of Engineering, Christian-Albrechts-University of Kiel, Kaiserstr. 2, 24143 Kiel, Germany

(Received 29 November 2012; accepted 22 January 2013; published online 11 February 2013)

The light-beam-induced current-based CELLO measurement technique (solar CELl LOcal characterization), originally developed for wafer-based silicon solar cells, can successfully be applied to thin-film solar cells, provided that contacting of a single cell is possible. This is shown exemplarily for several crystalline silicon on glass samples, having varying quality with respect to photocurrent extraction, series resistance, and power losses. For the latter, a comparison with results obtained from dark lock-in thermography gives quantitative agreement, provided that the cells are not severely shunted. © *2013 American Institute of Physics*. [http://dx.doi.org/10.1063/1.4790479]

I. INTRODUCTION

In order to fully understand the specific problems with any kind of solar cell, either under development or from production, a spatially resolved measurement is essential. The most important aspect is to identify reasons for power losses. This can be achieved using the spatially resolved solar cell measurement technique CELLO (solar CELl LOcal characterization), which is an advanced LBIC (light-beam-induced current) tool.[1] Originally developed for the analysis of wafer-based silicon solar cells, it was continuously improved over the years, especially concerning measurement speed and versatility.[2–5] At present, it has four different lasers which can scan confocally over the sample (smallest focus size: 50 μm). Since they range from blue (wavelength: 405 nm) over red (650 nm) to IR (850 nm and 934 nm, the latter called SIR: "stronger IR"), they have quite different penetration depths. All lasers can be modulated with different frequencies in the 10 kHz range, and the corresponding small-signal linear response is obtained by an *in situ* software lock-in using fast Fourier transform analysis, enabling a simultaneous measurement.

The solar cell is contacted with separate leads for current supply and voltage measurement, all connected to a very fast electronic feed-back for either potentiostatic or galvanostatic conditions. A global dc illumination, optimized for constant intensity, can be applied by halogen lamps (typically 0.3 suns so as not to overstrain the measurement electronics). The whole setup is time-calibrated so that both amplitude and phase (time offset between excitation and response) are measured. This makes possible not only very fast standard-LBIC-like scans at short-circuit conditions (a map of $\sim 10^6$ pixels takes roughly 15 min) but also maps of current or voltage response at arbitrary points of the illuminated *I–V* characteristic can be obtained.

Further information about the solar cell as, e.g., the series resistance (for which also the slope of the *I–V* characteristic at U_{oc} is needed),[6,7] possibly complemented by phase-shift maps,[4,8] or relative power losses at the maximum power point (mpp)[9] can be derived. Since ratios of amplitude maps are used for that the influence of laterally varying reflectivity is eliminated. Full short-circuit current data (amplitude and phase) from different lasers measured for different modulation frequencies can be fitted to the analytical solution of the 1D diffusion equation, yielding maps of secondary parameters like minority carrier lifetime τ, back surface recombination velocity S_b, minority carrier diffusion coefficient D, and $R_{ser}C$ time constant (local series resistance times local junction capacity).[3–5]

Except for the latter approach (that assumes photocurrent generation from diffusion in a wafer), all CELLO measurement and analysis concepts can be applied to all kinds of solar cells, since for the interpretation of the CELLO data no specific solar cell model is needed. Here, we present some possibilities to analyze thin-film solar cells by CELLO, exemplarily shown for samples cut from (legacy) crystalline-silicon-on-glass (CSG) modules.[10] These are chosen because they allow to demonstrate a variety of relevant aspects and because they allow a direct comparison with dark lock-in thermography (DLIT) results, obtained from the same samples.[11–13]

II. SAMPLES

The CSG module structure is schematically shown in Fig. 1. Active layer sections of 6 mm width form the equivalent of single cells (separated by the grooves). Alternating rows of 15 point contacts to the n^+- and p^+-Si layer (so-called craters and dimples, respectively) are linked on the back side by Al interconnection strips, each spanning two cells only (symbolized by the long blue/red bars in Fig. 1), which leads to a shunt-insensitive series connection in the module. Separate single-cell contacts (needed for the measurements) were prepared by evaporating a thin gold layer on the neighboring cells (symbolized by the yellow areas in Fig. 1) and using conductive adhesive tape.[11] We investigate samples from different production times ("old"[12] and "new"[11,13]), having specially treated glass surfaces for better light trapping ("abrade" or "beads") that lead to quite high short-circuit current densities.[14] Both the "old" and the "new" samples have previously been

[a]Author to whom correspondence should be addressed. Electronic mail: jc@tf.uni-kiel.de.

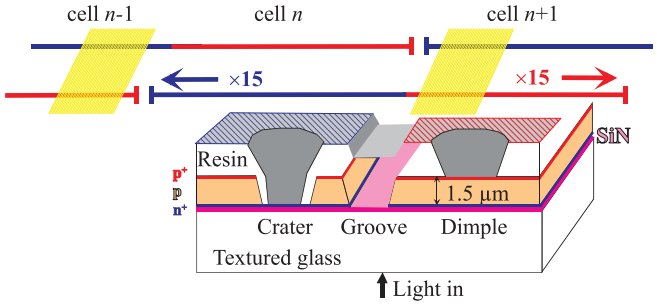

FIG. 1. CSG module structure (schematically), including additional contact preparations for single-cell measurements on cell *n*. The grooves, also being filled with resin, separate individual cells of 6 mm width. The cells are connected in series by Al strips, shown in gray. The blue/red hatching indicates the layer type (n^+/p^+) that the respective strip part is connected to by the craters/dimples (15 of each type per strip). The Al strips, each spanning two cells, are symbolized by long blue/red bars in the upper part; these bars show the Al strip arrangement typical for the CSG module structure. The yellow hatching symbolizes the gold layers applied for separately contacting cell *n*.[11]

studied by DLIT,[11–13] revealing groove shunts as the main loss mechanism. Incidentally, the contacting scheme originally developed for the CSG modules is now employed for laser-crystallized Si thin-film solar cells on glass under development by Suntech in collaboration with UNSW, Australia.[15]

III. RESULTS AND DISCUSSION

A. Spectral variation of the current response

Measured with a small reverse bias applied (typically −300 mV), the CELLO current maps dI_{rev} mainly show the full photocurrent response. In general, the dI_{rev} amplitude maps show inhomogeneities due to varying effective minority carrier lifetime or optical losses (as from reflectivity or absorbance in the active region); they correspond to standard-LBIC-like measurements but with suppressed series resistance influence. Figure 2 qualitatively compares dI_{rev} maps taken by different lasers for the same part of an "old" beads and an "old" abrade sample. Since in the CSG modules the n^+-Si layer is located close to the glass, the positions of the point contacts to the n^+-Si layer are visible in all maps; in the map of the blue laser (top in Fig. 2), they are the only ones visible. Rows of point contacts of the same type have a distance of 1 mm, giving the maps an intrinsic scale. The p^+-Si layer point contacts as well as some spots with reduced photocurrent production become visible only with increasing wavelength; this enables one to localize them at the back side of the active layer. Additionally, Fig. 2(b) demonstrates that some "large-scale" features of reduced photocurrent generation may become less and less visible with increasing wavelength, allowing to localize them at the front side of the active layer. They are faintly visible also in the relevant phase maps (not shown), indicating that these structures are more than just reflectivity variations (possibilities: n^+-Si layer property or injection-level dependence).

Most decisive for the front/back side feature distinction is the map of the blue laser. As the active layer of the CSG modules is just 1.5 μm thick, the differences in the red and SIR laser maps are mainly related to the light trapping properties of the respective CSG sample.

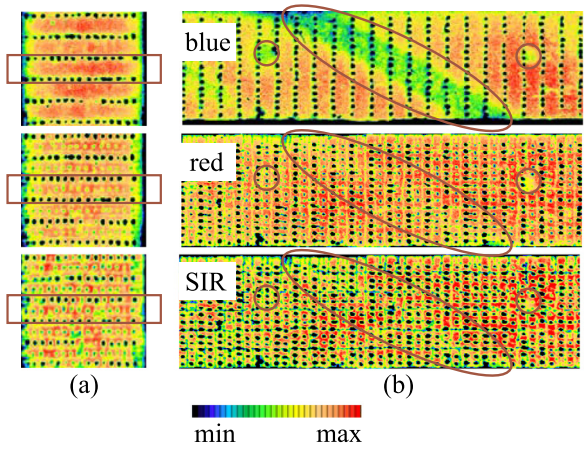

FIG. 2. Current amplitude maps measured at a bias of −300 mV, dI_{rev} (qualitatively; the color scale holds for all maps). From top to bottom: maps of the same part of the sample, taken by the blue/red/SIR laser; 40 pixel/mm. Point contact rows of the same type have a distance of 1 mm. Note the different sample orientations in (a) and (b). (a) Old beads-textured sample. In the center of the rectangular marks a row of p^+-Si layer point contacts is found, becoming visible only with increasing wavelength. (b) Old abrade-textured sample. The marks refer to current loss features that become less and less visible with increasing wavelength.

B. Current response at short circuit and under reverse bias

CELLO measures the short-circuit current response dI_{sc} potentiostatically at 0 mV reference voltage. Inhomogeneities in the ratio map dI_{sc}/dI_{rev} point to areas possibly containing ohmic shunts, a bad diode quality (low effectiveness of charge separation), or increased series resistance; the defect type cannot be identified just from this ratio map. Figure 3 presents such maps of an old and a new beads-textured sample. The old beads-textured sample (identical section as in Fig. 2) shows an inhomogeneous and significantly reduced overall current response, most likely due to preparation artifacts leading to imperfect single-cell contacts having high series resistance. This prevents the photocurrent from being fully extracted. However, also intrinsic losses become visible, most prominent around the (left and right) cell edge, indicating the presence of at least one of the aforementioned problems (shunt/bad diode/series resistance) near the grooves; the position of a broken Al interconnection strip

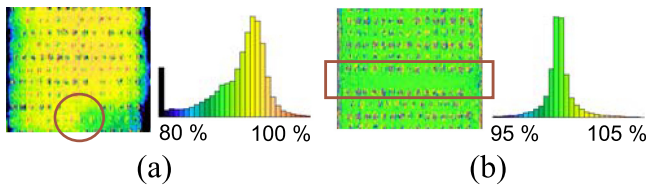

FIG. 3. Short-circuit current response of the SIR laser normalized to the reverse-bias photocurrent, dI_{sc}/dI_{rev}, giving the fractional current response under short-circuit condition (quantitatively); 40 pixel/mm. In these ratio maps, the values at the contact holes and the cell edges (grooves) are dominated by noise (partly eliminated; set to grey). (a) Old beads-textured sample, same cell area as in Fig. 2(a): significantly reduced and inhomogeneous current output, position of broken Al interconnection strip marked. (b) New beads-textured sample: much more homogeneous and much better overall current extraction than for the "old" sample (note the different scales), one row of p^+-Si layer point contacts missing (marked).

(as known from visual inspection using a microscope) is marked in Fig. 3(a). In contrast, the new beads-textured sample shows a quite homogeneous current extraction ratio of nearly 100%. The missing row of p^+-Si layer point contacts [marked in Fig. 3(b)] does not lead to a reduction of the extracted current. These observations imply that for this sample the external contacts are much better.

C. Current loss at maximum power point

Under operation, the current output at mpp is essential. Measuring the relevant current response, dI_{mpp}, and normalizing it to the reverse-bias photocurrent, dI_{rev}, shows current losses reducing the efficiency of the solar cell. Figure 4 shows dI_{mpp}/dI_{rev} maps taken with the SIR laser for (a) the old and (b) the new beads-textured sample (same areas as in Fig. 2). In Fig. 4(a) stripes and halos with increased values around the p^+-Si layer point contacts are prominent (see arrows), which means that the distance the current "travels" to reach the p^+-Si layer point contacts is critical. This demonstrates that despite the external contacting problems a detrimental intrinsic limitation is identified for this cell. In Fig. 4(b), the missing p^+-Si layer point contact row as well as the (left and right) cell edges shows up as main loss areas. As long as relatively few point contact rows are missing, only the edge loss is serious since it reduces the active cell area globally. This loss was not visible in Fig. 3(b), which enables one to relate it to a nonlinear shunt or to series resistance influence.

D. Series resistance from open-circuit voltage maps

CELLO measures the open-circuit voltage response dU_{oc} galvanostatically at 0 mA external current, i.e., the whole photocurrent generated cannot leave the cell. The linear-response voltage signal measured at the reference electrodes for local laser illumination scales with the locally generated photocurrent, and the accordingly normalized map dU_{oc}/dI_{rev} shows mainly series resistance effects. From this map and the slope of the *I–V* characteristic at U_{oc}, a series resistance map is calculated.[6,7] The R_{ser} results for the old and new beads-textured sample are shown in Fig. 5. The former shows much higher values than the latter which is due to the bad contact quality. From separate CELLO measurements, it

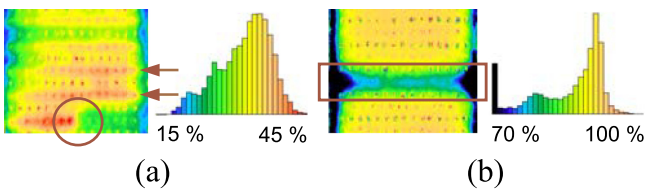

FIG. 4. Current response of the SIR laser at mpp normalized to the reverse-bias photocurrent, dI_{mpp}/dI_{rev}, giving the fractional current response at mpp (quantitatively; note the different scales); 40 pixel/mm. (a) Old beads-textured sample, same area as in Figs. 2(a) and 3(a): massively reduced current output, series resistance effect of broken Al interconnection strip visible (marked); general feature: stripes and halos around p-layer contact holes (arrows). (b) New beads-textured sample, same area as in Fig. 3(b): much better overall and much more homogeneous current extraction than for the "old" sample; one row of p contacts missing (marked); general feature: decay towards the (left and right) cell edges.

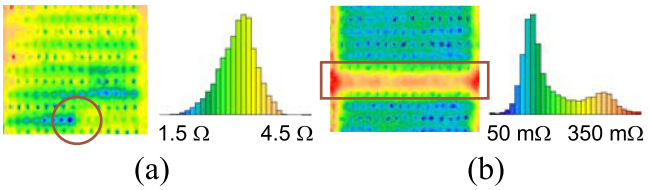

FIG. 5. CELLO series resistance maps, obtained from open-circuit voltage maps normalized to the reverse-bias photocurrent, dU_{oc}/dI_{rev}, according to Refs. 6 and 7; SIR laser, 40 pixel/mm. (a) Old beads-textured sample, same area as before: halos and stripe pattern around p^+-Si layer contacts, broken Al strips visible (marked). (b) New beads-textured sample, same area as before: much less pronounced stripe pattern, missing row of p^+-Si layer point contacts with significantly higher values (marked); also higher values towards the cell edges.

is known that the global R_{ser} variation of the old beads-textured sample visible in Fig. 5(a) is due to an artifact from the preparation of the external contacts. Nevertheless, in Fig. 5(a) the stripe and halo pattern known from Fig. 4(a) is unambiguously identified as a series resistance effect: Currents flowing through the p^+-Si layer lead to voltage losses reducing the current extraction from parts further away from the p^+-Si layer point contacts. The sheet resistivity of the p^+-Si layer is much higher than that of the n^+-Si layer,[12] which explains the asymmetry between the behavior of the n^+- and the p^+-Si layer. For the new beads-textured sample, increased series resistance is only found for the missing row of p^+-Si layer point contacts and towards the (left and right) cell edges.

E. Relative power loss and comparison with DLIT

To numerically evaluate the influence of current and voltage losses occurring at mpp, one can determine the relative improvement obtained for the (hypothetical) case that the whole cell behaved as its best part. Expressed as relative power loss, this can be obtained in linear order in the following way:[9]

$$\frac{\Delta P}{P} = \frac{\Delta\langle dI_{rev}\rangle}{\langle dI_{rev}\rangle} + \frac{\Delta\langle dI_{mpp}/dI_{rev}\rangle}{\langle dI_{mpp}/dI_{rev}\rangle} + \frac{\Delta\langle dU_{mpp}/dI_{rev}\rangle}{\langle dU_{mpp}/dI_{rev}\rangle}. \quad (1)$$

Here, the arrow brackets indicate the mean value of the respective map, and the delta sign refers to the difference between the mean values of the whole cell and of its best part. This is illustrated in Fig. 6 for the new beads sample, where only a certain section having good external contact quality is considered. The best part of this section obviously is the vertical center strip (one-third of the total cell area used), which is separately displayed in Fig. 6(b) to provide the relevant average value. Thereby, whatever mechanism leads to power loss at the cell edges (shunt or series resistance) is effectively removed.

The total relative improvement according to Eq. (1) amounts to $(30.14-29.31)/29.31+(910.2-880.2)/880.2+(7764-7516)/7516=2.8\%+3.4\%+3.3\%=9.5\%$, which for a given efficiency of 6.5%[13] gives an increase of 0.62% absolute. Considering only the mpp contributions, the relative improvement would be 6.7%, corresponding to an efficiency increase of 0.44% absolute. Both values compare very well

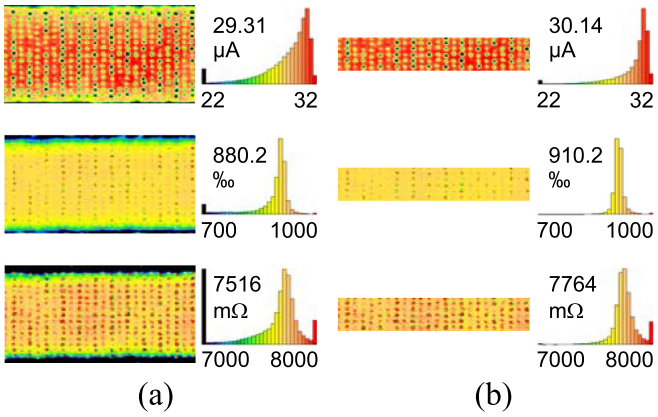

FIG. 6. Representative areas of the new beads-textured sample used for calculating the relative power loss according to Eq. (1), mean values and units of measure given at the histogram; from top to bottom: dI_{rev}, dI_{mpp}/dI_{rev}, dU_{mpp}/dI_{rev}, SIR laser, 40 pixel/mm. (a) Average values taken over the whole cell section, providing the reference values. (b) Average values taken over the center area (vertically, one-third) only, providing the values of the best parts.

with the DLIT result of 0.44%.[11,13] An analogous procedure yields for the new abrade-textured sample a total relative improvement of 1.7% + 4.9% + 4.6% = 11.2%, which for a given efficiency of 7.13%[13] gives an increase of 0.80% absolute. This is smaller than 1.34% as determined by DLIT.[11,13] Remembering that Eq. (1) holds only up to linear order, while the DLIT result is based on a simulation taking all nonlinearities into account, it is clear that for larger power losses Eq. (1) will give a smaller value. The reason for the larger losses occurring for the new abrade-textured sample most probably is that it is shunted much stronger[11] so that the average CELLO values of the best parts might already be affected by the shunt.

IV. SUMMARY

In summary, we have demonstrated the successful application of CELLO measurement and analysis procedures to crystalline-silicon-on-glass thin-film solar cells. Both optical and electrical properties were investigated qualitatively and/or quantitatively, namely spectral variation of the photocurrent, photocurrent extraction, series resistance, and power losses at maximum power point. The latter results agree very well with previous DLIT analyses. Altogether, this shows CELLO's capability to come to an extensive evaluation of limiting factors for and possible improvements of thin-film solar cells.

ACKNOWLEDGMENTS

We thank J. Schneider (CSP Halle, Germany; formerly with CSG Solar, Germany) and H. Straube (Jenoptik AG, Germany; formerly with MPI Halle, Germany) for providing the samples and for valuable discussions. This work was supported by the Deutsche Forschungsgemeinschaft under Contract No. FO 258/11-2.

[1]J. Carstensen, G. Popkirov, J. Bahr, and H. Föll, Sol. Energy Mater. Sol. Cells **76**, 599 (2003). CELLO is commercially available from ET&TE GmbH, Germany.
[2]J. Carstensen, A. Schütt, G. Popkirov, and H. Föll, in Proceedings of 21st European Photovoltaic Solar Energy Conference, 2AO.3.4, Dresden, 2006.
[3]A. Schütt, S. Keipert, J. Carstensen, and H. Föll, in Proceedings of 22nd European Photovoltaic Solar Energy Conference, 1CV.1.35, Milan, 2007.
[4]J. Carstensen, A. Schütt, and H. Föll, in Proceedings of 23rd European Photovoltaic Solar Energy Conference, 1AO.6.1, Valencia, 2008.
[5]J. Carstensen, A. Schütt, G. Popkirov, and H. Föll, Phys. Status Solidi C **8**(4), 1342 (2011).
[6]J. Carstensen, A. Schütt, and H. Föll, in Proceedings of 22nd European Photovoltaic Solar Energy Conference, 1CV.1.34, Milan, 2007.
[7]J. Carstensen, A. Abdollahinia, A. Schütt, and H. Föll, in Proceedings of 24th European Photovoltaic Solar Energy Conference, 1CV.4.33, Hamburg, 2009.
[8]J. Carstensen, A. Schütt, A. Pape, and H. Föll, in Proceedings of 25th European Photovoltaic Solar Energy Conference, 2CV.3.19, Valencia, 2010.
[9]J. Carstensen, S. Mathijssen, G. Popkirov, and H. Föll, in Proceedings of 20th European Photovoltaic Solar Energy Conference, 1AV.2.40, Barcelona, 2005.
[10]M. A. Green, P. A. Basore, N. Chang, D. Clugston, R. Egan, R. Evans, D. Hogg, S. Jarnason, M. Keevers, P. Lasswell, J. O'Sullivan, U. Schubert, A. Turner, S. R. Wenham, and T. Young, Sol. Energy **77**, 857 (2004).
[11]H. Straube, J.-M. Wagner, J. Schneider, and O. Breitenstein, J. Appl. Phys. **110**, 084513 (2011).
[12]H. Straube, O. Breitenstein, and J.-M. Wagner, in Proceedings of 24th European Photovoltaic Solar Energy Conference, 3AV.1.7, Hamburg, 2009.
[13]H. Straube, "Quantitatives Verständnis von Lock-in-Thermographie an Dünnschicht-Solarmodulen," Ph.D. thesis (Martin-Luther-Universität Halle-Wittenberg, 2011).
[14]M. J. Keevers, T. L. Young, U. Schubert, and M. A. Green, in Proceedings of 22nd European Photovoltaic Solar Energy Conference, 3DP.2.3, Milan, 2007.
[15]J. Dore, R. Evans, U. Schubert, B. D. Eggleston, D. Ong, K. Kim, J. Huang, O. Kunz, M. Keevers, R. Egan, S. Varlamov, and M. A. Green, "Thin-film polycrystalline silicon solar cells formed by diode laser crystallisation," Prog. Photovoltaics (published online).